Materials Characterization 192 (2022) 112198

Contents lists available at ScienceDirect

Materials Characterization

journal homepage: www.elsevier.com/locate/matchar

Digital fingerprints of microstructural variation in titanium alloy hip joint forgings via machining force feedback analysis

Beatriz Fernández Silva [a], Daniel Suárez Fernández [a,b], Ivan Green [c], Martin Jackson [a,*]

[a] Department of Materials Science and Engineering, University of Sheffield, Sir Robert Hadfield Building, Mappin St, Sheffield S1 3JD, UK
[b] Advanced Manufacturing Research Centre, Advanced Manufacturing Park, Catcliffe, Rotherham S60 5TZ, UK
[c] JRI Orthopaedics, 35A Business Park, 18 Churchill Way, Sheffield S35 2PY, UK

ARTICLE INFO

Keywords:
Microstructure
Texture
Titanium
Forging
Processing
Machining

ABSTRACT

Considering actual trends regarding life expectancy, it is forecast that the total number of hip replacements will increase in the next few decades due to an increasingly ageing population. This situation will require an increase in component supply and experience of titanium alloy closed-die forging experience in the manufacturing supply chain. However, the scrutiny of microstructural evolution during processing for orthopaedic implants is not at the same level compared to the aerospace industry. This study is focused on understanding the current microstructure quality in the international forging supply chain by applying standard characterisation techniques, currently used in the aerospace industry for safety critical titanium alloy components, as well as a Sheffield developed machining force feedback technique. Three different manufacturers whose near net shape hip joint forgings all successfully pass the industry standards were studied. Through digital fingerprint reconstructions, the microstructural variation has been shown to be linked to the forging process parameters which could help to determine the individual components' fatigue performance. Furthermore, significant variations have been identified in microstructure quality that could compromise the part performance. The study demonstrates that the materials standards for orthopaedic implants could be more stringent to avoid such large microstructural variations in the supply chain.

1. Introduction

Titanium orthopaedic parts are manufactured to very high standards with regard to chemical and biological compatibility for the use of in-vivo artificial internal implants. The design of such orthopaedic parts presents an extra set of technical challenges across different disciplines compared to aerospace titanium alloy components, such as chemical biocompatibility with the human body, mechanical-elastic compatibility with bone tissue, wear compatibility at the implant/tissue interface and ultimately the optimum adhesion of the implant. Good communication across the manufacturing supply chain is critical for the correct design, manufacture and service life of orthopaedic titanium implants.

Compared to Co-Cr and stainless steels, which have historically been used for biomedical components, titanium alloy implants are reported to last approximately 20 years with 95% of hip replacements lasting at least 10 years – making titanium the most suitable metal for implants [1]. The most common type of failure, accounting for ~42% of revision cases, is mechanical (aseptic) loosening with implant failures being far less common (~6%) [2]. Moreover, most implant failures, such as periprosthetic fractures, infection, dislocation or surgical technique error, are beyond the influence of the manufacturing process. However, the ongoing optimization of material and manufacturing processes for surgical implants, such as hip joints, is necessary to reduce or minimize revision cases. Furthermore, implant stem fracture can be caused by either poor primary proximal fixation by the surgeon or poor quality forgings. In 2016, approximately 100,000 primary hip replacement procedures were carried out in England, Wales and Northern Ireland, of which +6000 replacements may have been required due to implant failure [3](NJR, 2016).

The fatigue performance of titanium alloy components is well-understood to be related to the microstructure and crystallographic texture defined by the primary manufacturing processes. Although there are ASTM standards highlighting the microstructure and forging requirements [4,5], the minimum fatigue life requirements [6,7][ISO 7206-4:2010, ISO 7206-6:2013] and material specification [ISO 5832-3]

* Corresponding author.
E-mail address: martin.jackson@sheffield.ac.uk (M. Jackson).

https://doi.org/10.1016/j.matchar.2022.112198
Received 15 February 2022; Received in revised form 18 July 2022; Accepted 3 August 2022
Available online 6 August 2022

[8], currently the manufacturing and shaping route for titanium alloy hip joints is not specifically defined in the standard, which leads to inconsistencies in the method of manufacture between forging suppliers. Furthermore, the effect of crystallographic texture of hip joint components has largely been ignored, despite its strong influence on fatigue performance. In addition, recent research has shown the importance of the crystallographic texture in biomaterials on cell response [9], which could enhance osteogenesis and hydroxyapatite adhesion [1] and therefore, indirectly reduce the cause of revision for non-manufacturing processing effects.

In this study, the microstructure and crystallographic texture developed during the near net shape (NNS) hip joint manufacturing process is characterised for different forging manufacturers. The aim was to determine the impact of the thermomechanical processing variables used in the supply chain on the microstructural and crystallographic texture development that will define the in-service behaviour. The resolution of characterisation used in this study is usually performed in critical aerospace titanium alloy components, and therefore this work aims to highlight the current situation in the supply chain quality of such forged parts.

Although partial or total hip arthroplasty (THA) is a common intervention with high survival rates and low mortality rates: several issues can imply a revision and substitution of at least one component of the implant. These hip joints consist of four main components; the acetabular cup that sits in the acetabulum, the femoral head which can be ceramic or metallic, the plastic/ceramic liner that sits between the acetabular cup and the femoral head and finally the femoral stem (hip stem). The exploded CAD view of the main parts of a complete hip replacement orthopaedic implant is shown in Fig. 1.

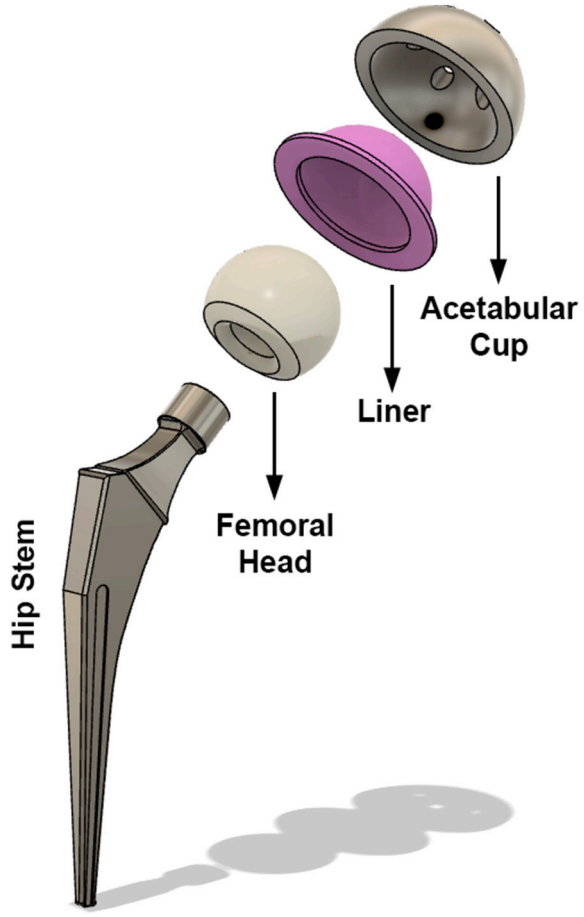

Fig. 1. Exploded CAD view of the four main components of a total hip arthroplasty (THA).

A study centred in more than 2000 THAs, performed in 30 centres in France, showed the causes of implant revision (implying that at least one part of the implant had to be replaced), with implant fracture being one of them [2].

The design and improvement of these orthopaedic implants is challenging, due to the lack of nationwide clinical databases and registers where important clinical data (about the failures and revisions) is collected and centralised. This makes it difficult to have statistical data at a national and international level regarding the success/failure ratio and specific data about the failure origin in THA surgical procedures. However, the creation and distribution of these data sets is challenging due to the sensitive information included about individual patients and the rigorous requirements to follow based on the legislation, such as the data protection laws such as the Data Protection Act 2018 in the UK [10]. Digitisation efforts are being put in place by government and healthcare institutions such as the NHS in England, creating a novel country-wide electronic health record for public research purposes [11].

This work addresses the inconsistencies in microstructure, crystallographic texture development and machining response in the current supply and manufacturing industry of orthopaedic hip joint femoral titanium components. A comprehensive characterisation of the material is performed using a similar approach to that used for critical aerospace components, presenting the relationship between the analysis results, the processing variables and ultimately, the component's performance.

2. Methodology

2.1. Sample description

A set of hip joint forgings originating from three different international forging manufacturers (coded A, B and C) were provided by JRI Orthopaedics Ltd. in Sheffield, UK. The hip joint forgings were taken from the process route prior to finish machining and coating, and therefore, the geometry and dimensions of the three forgings are identical. Importantly, all three hip joint forgings had successfully passed the standardised requirements, stated in the respective standards for orthopaedic implants ISO 7206-4: 2010 ('Distal fatigue testing of the femoral stem') [6] and ISO 7206-6: 2013 ('Neck fatigue testing of the femoral stem') [7]. These implants are intended to be "uncemented" and therefore they need to be surface prepared and coated in hydroxyapatite ($Ca_{10}(PO_4)_6(OH)_2$) for optimal bone-implant mechanical interaction. As the coating is applied via plasma spraying, which is a high energy-low temperature but highly localised process, the microstructure and crystallographic texture developments of these implants in its pre-coated state, are considered unaltered during the coating procedure as the titanium substrate does not exceed 150 °C [12]. Therefore, the results presented in this work can be extrapolated through to the coated in-vivo implanted condition.

The three hip joint forgings are made of the same titanium alloy - Ti-6Al-4 V ELI (grade 23) and referred to as Ti-64. "ELI" refers to *Extra Low Interstitials*, which implies a higher purity variant of the more commonly available Ti-6Al-4 V alloy (grade 5) with lower levels of tramp elements such as oxygen, iron and carbon. As a result, the Ti-64 ELI variant provides better ductility, excellent fracture toughness (even down to cryogenic temperatures) and enhanced corrosion resistance compared to Ti-64. It is therefore used in orthopaedic implants, surgical instruments, marine and cryogenic applications.

The chemical composition of the studied hip joint forgings is shown in Table 1. These forgings have also fulfilled the requirements of ISO 5832-3 ('*Implants for surgery — Metallic materials — Part 3: Wrought titanium 6-aluminium 4-vanadium alloy*') [8].

Fig. 2 shows the three hip joint forgings in the as-received condition. All forgings have equivalent geometries.

Table 1
Ti-6Al-4 V ELI composition limits [weight %](Grade 23) AMS 4981/ Timet Ltd.

Ti-64 ELI	Ti	Al	V	N	C	O	Fe	H	Ru	Residual elements (each)	Residual elements (total)
MAX	Bal	6.5	4.5	0.03	0.08	0.13	0.25	0.0125	–	0.1	0.4
MIN	Bal	5.5	3.5	–	–	–	–	–	–	–	–

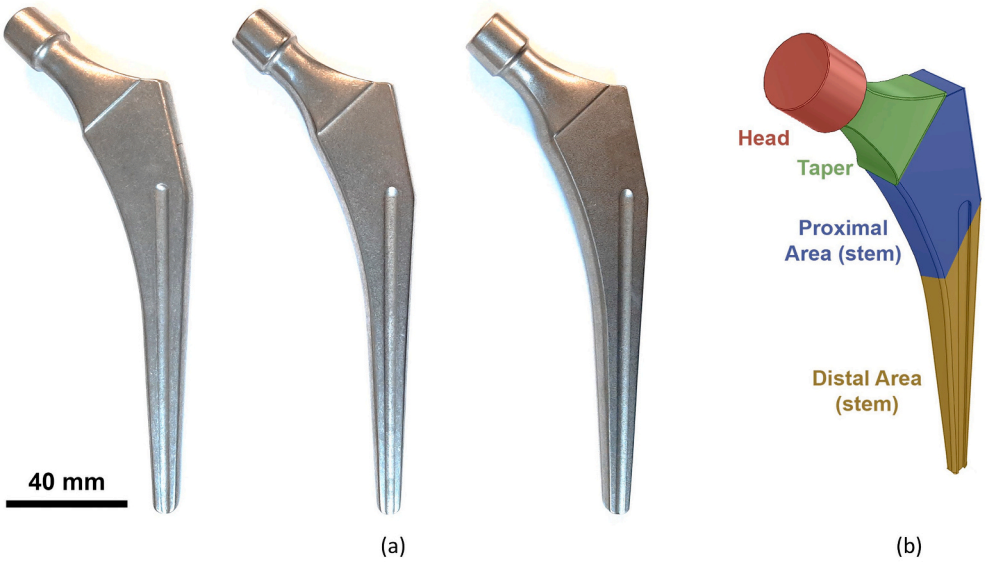

Fig. 2. Hip joint forgings from manufacturers A, B and C in the as-received (pre-finish machining) condition (a) and a schematic illustrating the four sections of a hip joint.

2.2. Sample manufacturing stages and reference axis

The current method of manufacturing this type of hip joint component (shown in Fig. 3) starts with a round Ti-64 ELI bar stock. In order to achieve the desired geometry, sequential forging and forming operations are applied to the Ti-64 ELI bar. First, due to the differences in geometry between the thin stem and the thicker top section of the final component (see Fig. 2(b)), the initial hot forming process reduces the diameter of the proto-stem part (Fig. 3(b)). The diameter reduction is less prominent at the opposite end, as more material is required for the forging of the head-taper region. This bar with sections of different diameters is then hot-formed to the designed angle of the final implant (Fig. 3(c),

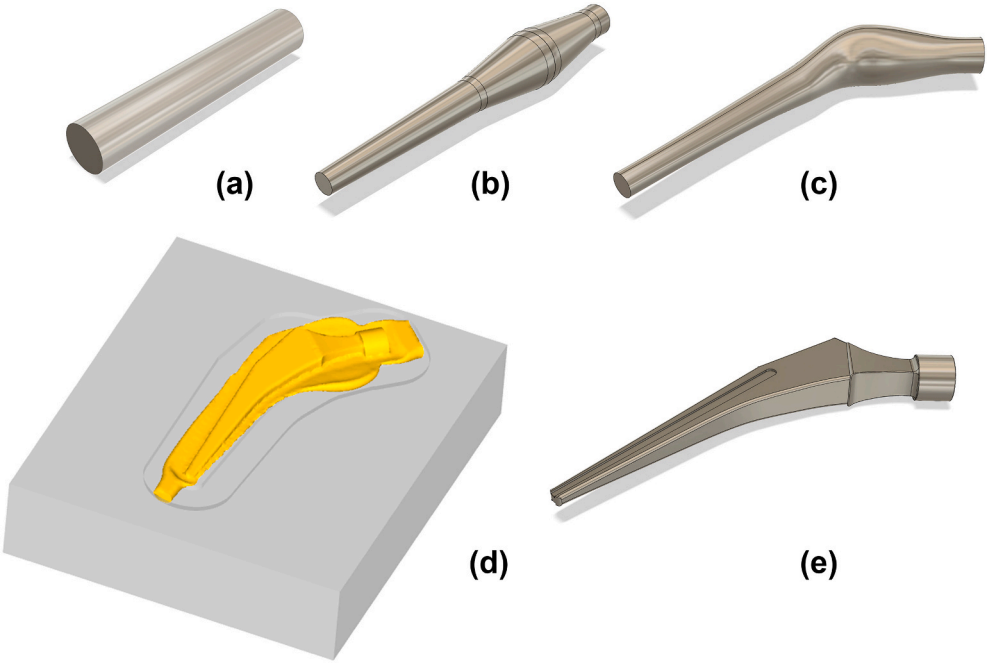

Fig. 3. The shaped profiles at each stage of hip joint forging and shaping route. Initial feedstock bar (a), local cross section reduction in stem region (b), femoral neck-shaft angle (NSA) (c), closed-die forging stage (d) and workpiece after machining in its pre-coating stage (e). The reference axes are shown at the bottom right.

preparing the part for the closed die forging process (Fig. 3(d), to form a final near net shape (NNS) with intricate features.

During these key manufacturing stages, processing parameters such as temperature, strain, strain rate and geometry determine the microstructural development, which ultimately defines the properties and the final component performance and quality.

The component reference axes used are kept constant for all stages of the analysis presented in this work: the axis RD is parallel to the longitudinal axis of the initial bar; the ND axis is normal to the plane defined by the closed-die forging process; and TD is the third spatial axis defined as the perpendicular direction to RD and ND. An overview of the shape evolution during the different forming stages of the manufacturing process, as well as the nomenclature of the reference axis, is represented in Fig. 3.

As pointed out by Behrens et al. [13], variations in the manufacturing route for these implants occur in the supply chain, depending on the optimising variable defined by the manufacturer (i.e. minimising material usage). As an example, either swaging, rotary forging or cross wedge rolling manufacturing processes can be used to achieve the intermediate geometry in step (b) of Fig. 3 from the initial bar (in step (a)). In this work, the RD axis will be referred to as the rolling direction, but it is unclear whether the first stage in the manufacturing process of the hip joints was performed by rolling or any other process, as highlighted above.

2.3. Sample extraction

The materials characterisation of these three components was carried out in two different locations. The microstructural and texture analysis was performed in the stem region, specifically at 80 mm from the end of the stem (Fig. 4). This location was selected as it is considered as a critical location in the standards applied for manufacturing and testing the validity of these biomedical implants (JRI Standards). The machining analysis was performed in the neck because it is an axisymmetric component that can be easily turned into a cylindrical piece.

The workpieces were sectioned in a Struers Secotom-50 with a 10S20 cut-off wheel of 200 mm diameter. The sectioning plan of each implant is depicted in Fig. 4.

From the slice extracted at 80 mm from the end of the stem, samples for light microscopy, microstructural analysis, hardness indentation and texture analysis were subsequently sectioned and metallographically prepared for microscopy.

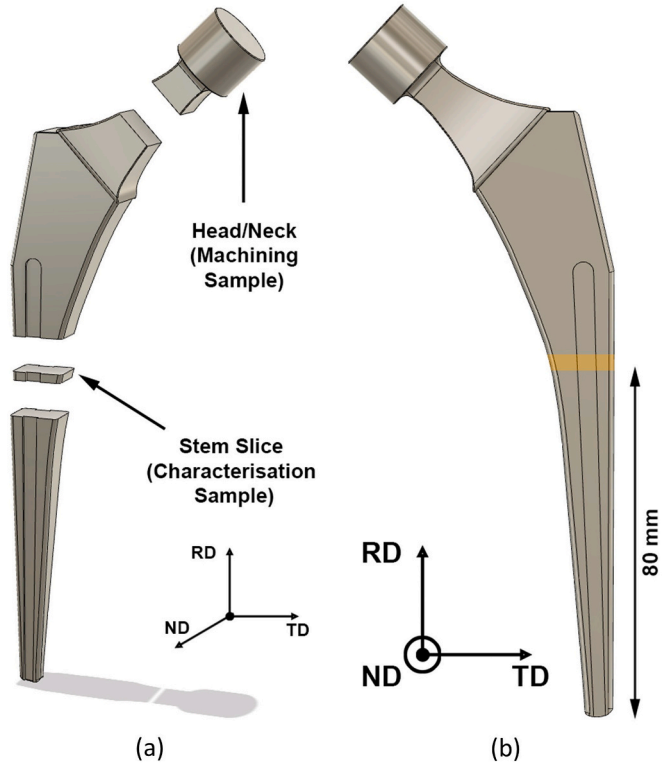

Fig. 4. Sample extraction from each workpiece characterisation slice and machining sample (a) and detail of the location of the stem characterisation slice, 80 mm from the end of the stem (b).

2.4. Materials metallographic characterisation

The three Ti-64 stem slices were prepared using standard metallographic procedures to obtain a mirror-like finished surface suitable for microstructure and texture analysis. The specimens were ground with SiC paper from 400 to 4000 grit size and polished for 15 min with colloidal silica 0.05 μm and 10% H_2O_2 followed by cleaning in an ultrasonic bath with isopropanol. For light microscopy and micro hardness measurements, the samples were etched using Kroll's reagent for 20 s. For scanning electron microscopy (SEM) and electron backscatter diffraction (EBSD), samples were analysed in the as-polished condition.

Light microscopy (LM) was performed under a Nikon LV150 light microscope and Clemex automated image analysis (Olympus Bx51 with Clemex Vision PE image software analysis system) for microstructure analysis. The crystallographic texture was obtained by EBSD in a JEOL JSM-7900F SEM equipped with a Symmetry detector coupled with AZtecHKL software for data collection and post processing was performed using MTEX [14]. Low resolution orientation maps were obtained covering areas of 300 × 1000 μm^2 using 1 μm step size. The analysis was performed on the TD-ND plane perpendicular to RD of the specimens as shown in Fig. 5. Two different locations were chosen: at the centre and at the edge.

The Vickers hardness was measured at each sample in the cross section from edge-to-edge at room temperature on as-polished and mounted specimens in a DuraScan microhardness tester. Tests were performed in accordance to the ASTM-E384 [15] specification under a force of 1 kg (HV1) for 15 s.

2.5. Machining force feedback analysis

The finish machining process is a dynamic interaction between the tool insert and the workpiece and it is used to remove material from the near-net shape forging until the final design geometry and tolerances are achieved.

The force feedback characterisation technique takes advantage of this dynamic interaction, providing an in-process analysis of the component's microstructure during the machining operation. This analysis is carried out using the machining forces exerted on the tool insert during the operation. These signals are subsequently evaluated and linked to the manufacturing process variables, material characteristics and ultimately with the unique quality of each machined component - and the basis of a "digital passport" of the hip joint. This is possible

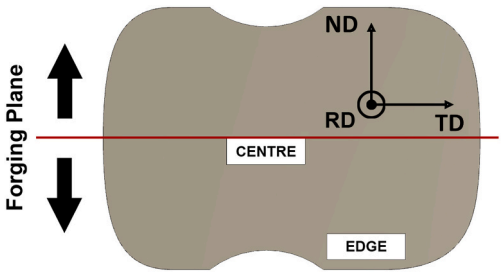

Fig. 5. Hip stem cross section representing the centre and edge locations in the TD-ND plane.

because machining can be considered a dynamic process, whereby severe plastic deformation exerted by a tool insert leads to intense shear banding and a controlled fracture at a specific subsurface depth (*depth of cut*), at a defined speed (*cutting speed*), and a fixed width (*feed rate*). As the material is being removed as chip/swarf through the machining process, the new surface created is representative of the final component material condition. Therefore, the data captured through this in-situ characterisation technique provides unique information about the specific component that is being machined.

The in-situ characterisation approach uses the forces exerted on a tool insert to determine the local material characteristics and the process dynamics. In order to capture such small variations in local machining forces, high precision piezoelectric sensors are housed inside a metallic plate (known as a dynamometer) that is mechanically attached between the tool holder and the CNC machine tool turret. The small capacitance variations are then amplified in a charge amplifier, discretised and then transferred via a USB link to a computer for further analysis.

The CNC centre used for this analysis was a DMG Mori NLX2500 at the University of Sheffield's Advanced Manufacturing Research Centre with Boeing, Rotherham, UK. The tool insert type used was a Sandvik VNGG 16 04 01-SGF H13A, uncoated with a tool corner radius of 0.0992 mm. The selection of an insert with a very small tool radius was because of the implicit reduction in surface contact area between the workpiece and the insert itself. This combined with very conservative machining parameters, drastically reduces the interaction volume in the subsurface layers and increases the number of points per unit area captured during the operation.

The main spindle chuck of the CNC centre is a SMW AUTOBLOK KNCS-M-210-52 and was equipped with three soft jaws model SMW AUTOBLOK WAK 200–10, providing the necessary clamping support for these small components. Soft jaws (of case hardened steel - 16MnCr5) were selected to avoid damage on the workpiece.

The dynamometer set up consists of a plate dynamometer (Kistler 9129AA) with eight piezoelectric sensors that measure the machining forces in the three spatial axes with two sensors measuring the forces in the X and Y axis respectively, and four separate sensors that combined measure the force in the Z axis.

The signal captured by the piezoelectric sensors [pC] is then transferred to the multichannel charge amplifier (Kistler Type 5070) through a Kistler 1677A high impedance reinforced cable connection and translated into Newtons of force. The multichannel charge amplifier output is then digitised and transferred to the computer using a data acquisition box (Kistler 5697A) and captured and exported using DynoWare software. The data gathered in each machining test was captured at an acquisition rate of 30 kHz.

A schematic of the dynamometer plate connected to the tool holder/insert and back plate, as well as the sensor position within the dynamometer plate, is shown in Fig. 6.

In order to perform the force feedback material analysis, the machining forces captured have to be transferred from the time domain to the 3D space. This is performed by parameterising the tool path in the time domain which creates 4D diagrams, where the fourth axis represents the local machining response using a colour scale. These diagrams were previously referenced as *fingerprint* diagrams [16,17]. The use of these diagrams presents a unique response per component that can be linked to the upstream manufacturing stages as well as, the individual components' performance and information about the process stability.

In this work, standard turning and face turning operations were performed in the sectioned hip joint necks from the three manufacturers under different machining conditions. The set of machining conditions used in these tests are summarised in Table 2.

The neck parts sectioned from the as-received hip joint forgings were pre-machined when fixed to the main spindle of the CNC machining centre, to ensure that the rotational axis of the machine and workpiece were parallel. Also, the smaller diameter region was extended to be able to maximise the outer diameter machining area. A schematic of the pre-machining operations carried out prior to testing is shown in Fig. 7.

3. Results

3.1. Microstructural characterisation of the Ti-64 hip joint forgings

The microstructural characterisation was performed in the three different hip joints from suppliers A, B and C in the plane perpendicular to rolling direction (RD) of the forgings, both at the centre and at the edge, as shown in Fig. 5. High magnification SEM images are shown in Fig. 8 for all specimens from the centre. Representative micrographs

Table 2
Summary of the machining parameters used for the force feedback analysis during the face turning and standard turning operations, respectively.

Face turning	ap [mm]	Feed [mm/rev]	RPM	Standard turning	ap [mm]	Feed [mm/rev]	Vc [m/min]
Test 1	0.05	0.01	605	*Test 1*	0.05	0.01	38
Test 2	0.1	0.01	605	*Test 2*	0.1	0.01	38
Test 3	0.05	0.08	605	*Test 3*	0.05	0.08	38
Test 4	0.2	0.08	605	*Test 4*	0.2	0.08	38

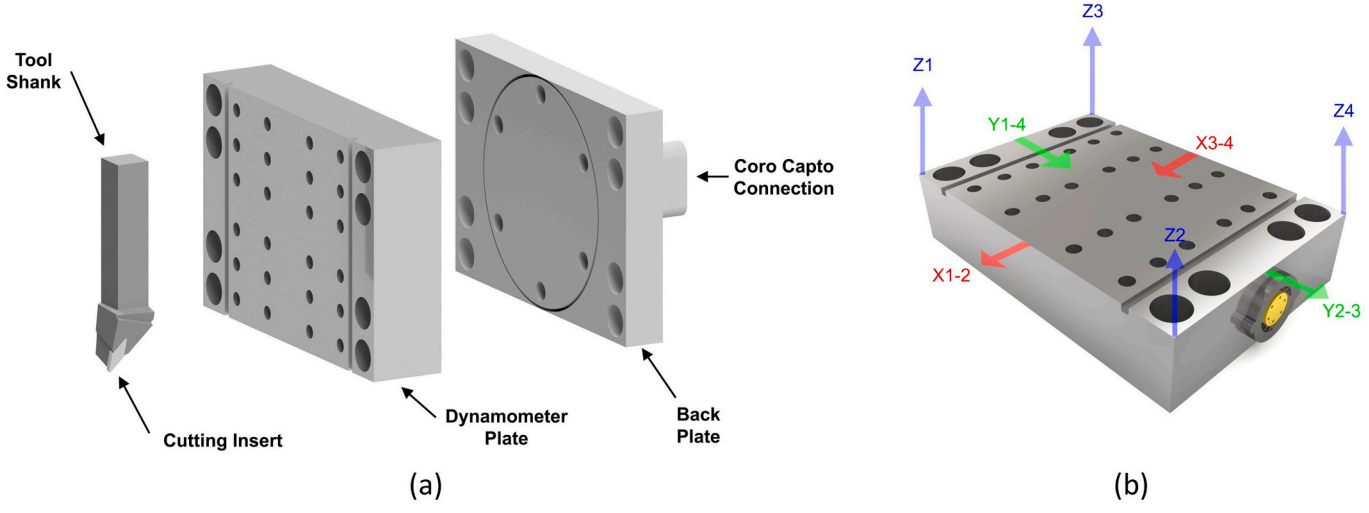

Fig. 6. Exploded 3D Schematic of the Kistler 9129AA dynamometer assembly (a) and sensor location within the dynamometer plate (b).

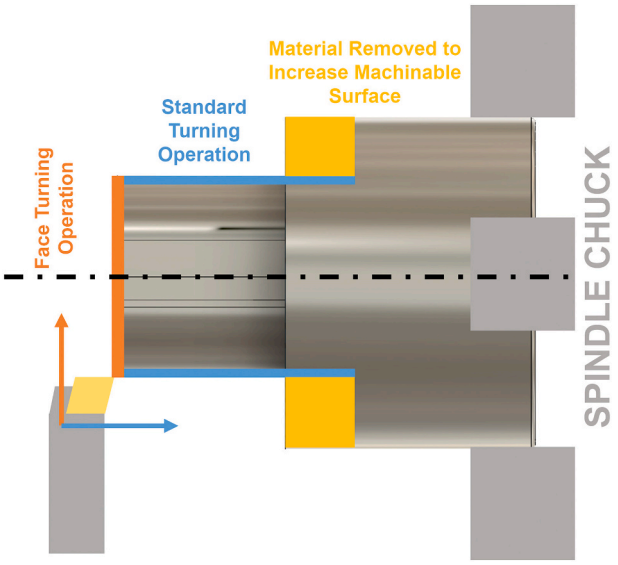

Fig. 7. Pre-machining operations applied to the sectioned neck region to ensure the workpiece surfaces were parallel with the machine axes.

from each sample are shown at both locations in Fig. 9. All specimens show a bimodal microstructure with a relatively high-volume fraction of primary alpha grains (α_p) within a transformed beta matrix of secondary alpha (α_s). Hip stem B has the lowest volume fraction of α_p with 51% (Fig. 8 (b)), while stems A and C have 63% and 69% of α_p grains, respectively (Fig. 8 (a, c)). Evidence of an alpha colony-lath microstructure is only observed in stem B (Fig. 9(b)) due to its lower volume fraction of α_p grains, while stem A (Fig. 9 (a)) followed by stem C (Fig. 9 (c)), reveal a microstructure consisting mainly of heavily interconnected α_p grains.

The average grain size diameter in all specimens is 6 μm with a mainly equiaxed morphology, creating agglomerates of several α_p grains, particularly in locations close to the edge. However, for stem B (Fig. 9 (b, e)) and stem C (Fig. 9 (c, f)), the microstructure is homogeneous with no major differences in morphology between the edge and centre locations. A heavily deformed microstructure was observed at the centre of stem A, shown in Fig. 9 (d).

The microstructure was also analysed throughout the whole cross-section in the RD plane. Stems B and C (Fig. 10 (b,c)) have an homogeneous distribution of grain size and morphology across the whole section - this was observed during the higher magnification analysis (Fig. 9 (b, e) and (c, f)). However, stem A shows stronger microstructural differences between the edge and the centre of the sample, Fig. 9 (a, d). The microstructure at the centre consists of heavily deformed and agglomerated α_p grains which create a band parallel to the TD direction and perpendicular to the closed-die forging axis, as shown in Fig. 10 (a). The microstructure of the centre region of stem A with elongated grains is shown in Fig. 9 (d).

3.2. Hardness analysis

The average hardness values for specimens A, B and C are shown in Fig. 11. These were obtained by averaging a total of 27 indentations obtained across the RD plane in the ND direction, being 320.6 ± 16.3 HV1, 339.0 ± 12.0 HV1 and 331.9 ± 11.8 HV1, respectively. Fig. 11 shows the value of each single indentation and its relative position along the stem cross-section. Despite the similarities in the average values between the three stems, stem A presents a significant variation in the measurement within the edge-to-centre section from 300HV1 to 362HV1, with the highest value coinciding with the plastic instability feature at the centre of the stem in Fig. 10(a). Stems B and C, however, showed relatively consistent hardness levels from edge-to-edge.

3.3. Texture analysis

The inverse pole figure (IPF) orientation maps regarding RD are shown in Fig. 12. These were obtained from the centre and the edge locations of each stem (Fig. 5). The basal and prismatic pole figures from the {0002} basal plane, the $\{10\bar{1}0\}$ prismatic plane and the $\{1\bar{2}10\}$ plane are shown in Fig. 13. Note that for stem A, the position of the orientation map was captured at a centre location where the intense plastic instability (observed in Fig. 10) was not present. This is evidenced by the lack of deformation in the microstructure, Fig. 12 (a) compared to the microstructure observed in Fig. 9 (d). Furthermore, the intense plastic instability defect is not a straight line from parallel to the TD.

The orientation maps show a relatively strong texture with significant variation between the centre and the edge locations. A strong prismatic texture is present at the edge locations with respect to RD (as shown in Fig. 12 (b, d, f)) where the c-axis of the HCP crystal is strongly aligned with ND (Fig. 13 (b, d, f)) being the main texture component $\{0002\}\langle 10\bar{1}0\rangle$ for stems A and B, and a stronger {0002} basal texture is

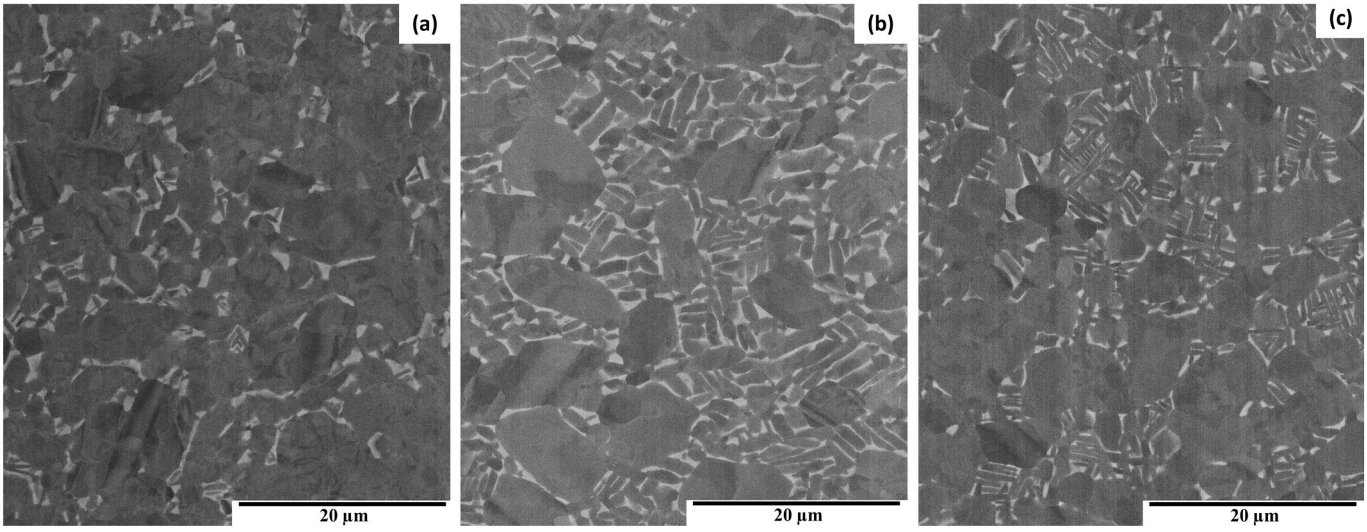

Fig. 8. Scanning Electron Microscopy micrographs of the Ti-64 microstructures of the stems from manufacturers (a) A, (b) B and (c) C.

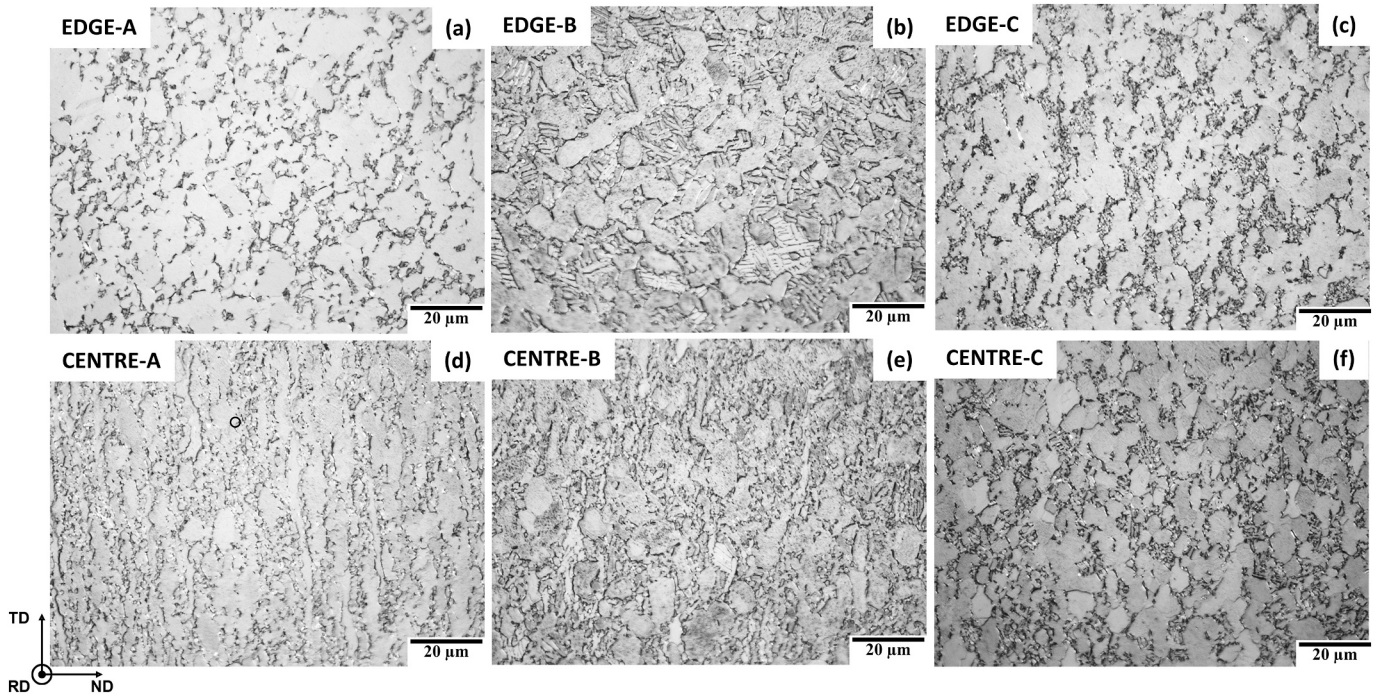

Fig. 9. Light micrographs of the Ti-64 microstructures at the edge (a–c) and centre (d–f) locations of the stems (from manufacturers A, B and C) cross-section in the RD plane.

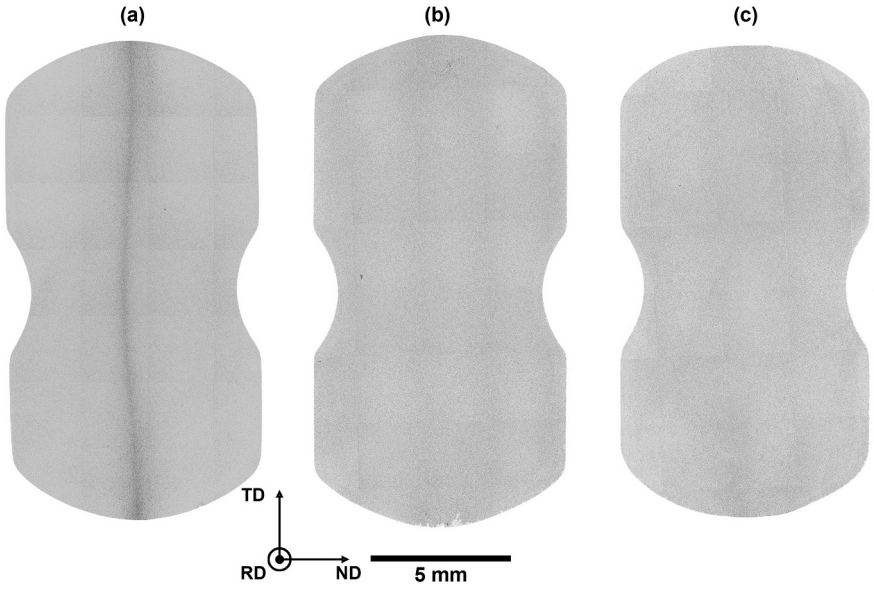

Fig. 10. Microstructure of the whole stem cross section in the RD plane from suppliers (a) A, (b) B and (c) C.

measured for stem C with even distribution of the prismatic planes around the RD-TD plane. This can be observed in the pole figures which represent the distribution of orientations of the crystallographic planes in a stereographic projection considering the projection axis of the sample TD, ND and RD. The pole figures at the edge of each stem (Fig. 13 (b, d, f)) show the conventional rolling texture in HCP crystals, where the c-axis is aligned with ND ({0002}//ND), displayed by the strong pole at the centre. Stems B (Fig. 13 (d)) and C (Fig. 13(f)) also show a weak pole in the RD, as a result of a higher volume fraction of transformed beta phase. This was not present in stem A where only the alpha phase belongs uniquely to the α_p grains. The strength of the rolling texture is described by the mrd (multiples of random distribution) values of approximately 4 times for stems A and B and more than double for stem C.

A stronger basal texture is generated towards the centre of the stems (Fig. 12 (a, c, e)). The strong rolling texture previously observed at the edge is weakened towards the centre of stems A and B, leading to a TD-split basal texture (Fig. 13 (a, c)). In stem C, the material texture undergoes a 90° lattice rotation (Fig. 13 (e)) leading to the c-axis of the HCP crystal being preferentially aligned with RD developing a texture component $\{11\bar{2}0\}\langle 10\bar{1}0\rangle$ in ND.

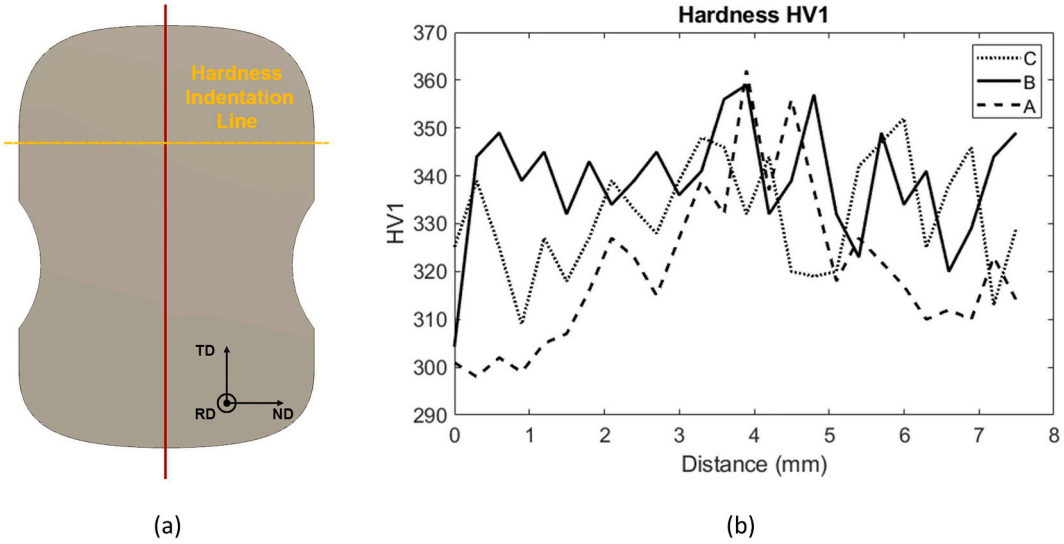

Fig. 11. (a) Hardness indentation line parallel to ND in relation to the cross-section position and the main axes and (b) Vickers Hardness indentations values on the RD plane from each specimen regarding its location from edge to edge.

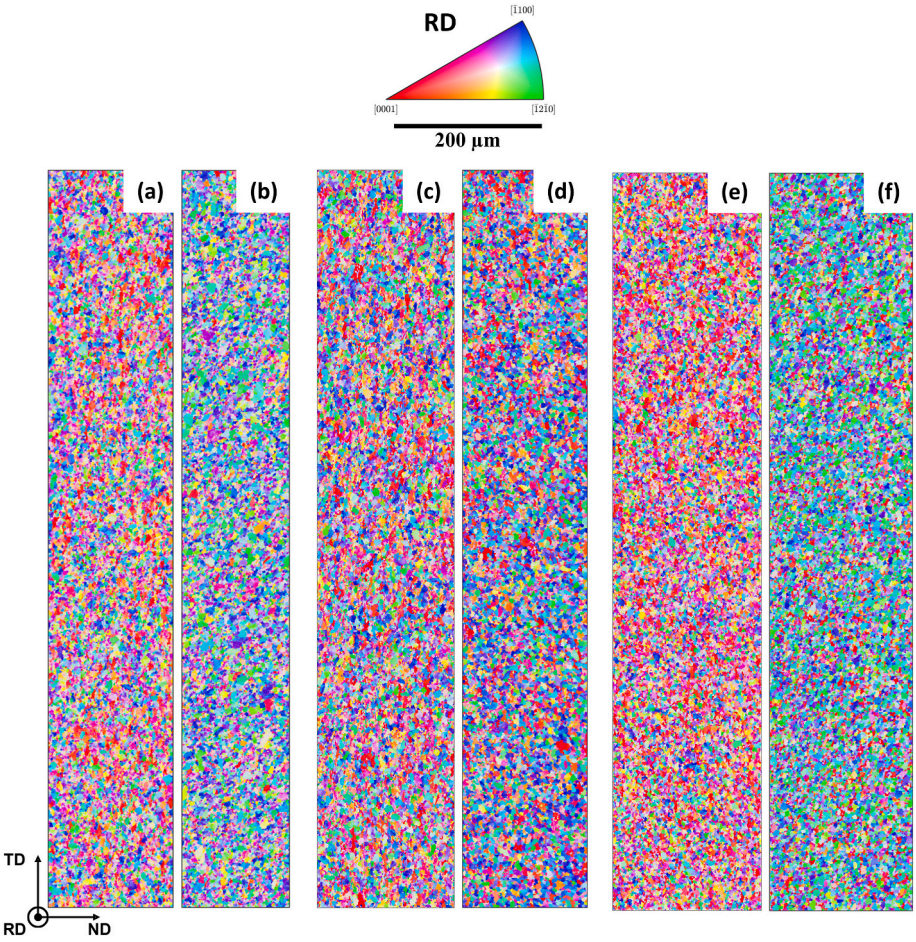

Fig. 12. IPF orientation maps regarding RD from stem A (a, b), stem B (c, d) and stem C (e, f) from centre (left) and edge (right) locations respectively. Note that the orientation map at the centre location in stem A is not in the plastic instability region.

3.4. Machining force feedback analysis

Two different machining operations were performed on the hip joint neck workpieces: a face turning operation, where the cross section of the sample is machined and a standard turning operation on the outer diameter. This was conducted in order to maximise the surface area that can be characterised and to analyse the machining response of the material in different orientations. In addition, these two machining

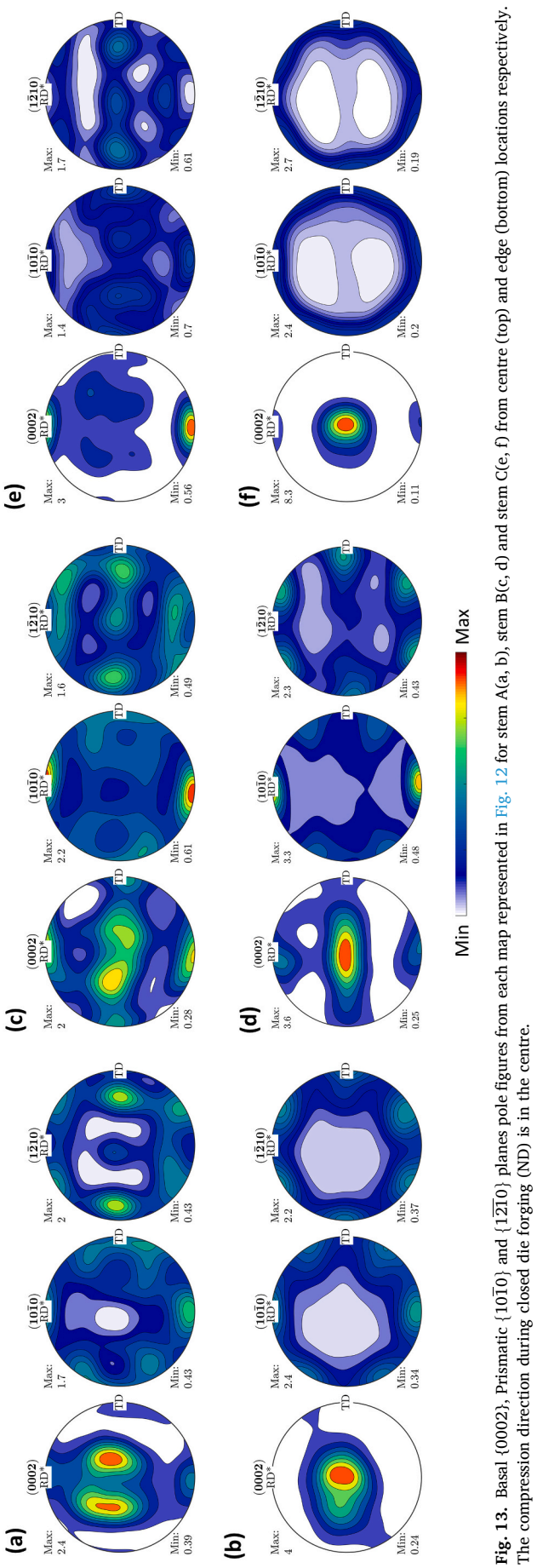

Fig. 13. Basal {0002}, Prismatic {10$\bar{1}$0} and {1$\bar{2}$10} planes pole figures from each map represented in Fig. 12 for stem A(a, b), stem B(c, d) and stem C(e, f) from centre (top) and edge (bottom) locations respectively. The compression direction during closed die forging (ND) is in the centre.

operations present their own characteristics. A standard turning operation is performed at a constant distance from the rotational axis of the component, and therefore a constant cutting speed and feed is maintained during the complete machining operation. This implies that the cutting behaviour of the material will be more homogeneous during the test. On the contrary, during a face turning operation, the distance between the point that is being machined and the rotational axis diminishes with time. In the set up used, a fixed RPM value was established during the complete test, to avoid a consistent movement of the tool towards the centre and to avoid an accelerating spindle speed. An accelerating spindle presents a challenge for force synchronisation in the spatial domain, due to the reaction time of the controller-kinematic system of the machining CNC centre.

3.4.1. *Statistical analysis of machining force data*

A statistical analysis was carried out on the three spatial axes measured per machining test and manufacturer. The signal from the standard turning trials was selected for this statistical analysis due to the consistency of the machining conditions during the operation. In this statistical analysis, the average machining force per axis was measured as well as the coefficient of variation. The average cutting force is a key factor to evaluate the machinability of a component and it is clearly linked to the (1) tool life; (2) machining conditions and (3) workpiece microstructure [18,19]. The coefficient of variation is a variable that benchmarks the stability of the cutting process under a common reference frame.

The coefficient of variation is calculated as the ratio between the standard deviation and the average value of the signal. This variable simplifies the comparison between the signals, understanding their differences and linking such differences to the material properties of the workpiece. The data used for the statistical analysis consists of the steady state cutting region of the signal, to avoid abrupt changes in the machining forces signal arising from the engagement and disengagement regions of the machining operation. The three forces captured by the 8 dynamometer channels are labelled as FF (feed force) as the force parallel to the feed axis, FL (longitudinal force) as the force parallel to the rotation axis of the sample, and FC (cutting force) as the force exerted on the insert in the cutting direction.

Fig. 14 shows the average signal value, and coefficient of variation per machining parameters used and axis. In the case of the average machining force, regardless of the machining parameters, specimen B presents a consistent higher average value. The largest difference between specimen B and the other suppliers, is shown when the uncut chip area is the smallest (Fig. 14 (a)). However, when the material removal rate increases, the differences between the three manufacturers are reduced.

However, when calculating the coefficient of variation, it is easier to compare how the signals fluctuate with respect to the average machining force measured per set of machining parameters and manufacturer. Specimen A presents the highest value of all three suppliers, where the values for the depth of cut and feed are the smallest, followed by specimens C and B. This trend is then inverted when the machining parameters are closer to the standard finishing operations for Ti-64 (Fig. 14(d)). These results are influenced by the chip that is generated, pinning down the insert through its rake face towards the material, reducing vibration and enhancing the stability of the process [20]. The authors consider that this is the reason behind the reduction in coefficient of variation when increasing the uncut chip area.

3.4.2. *Outer diameter (OD) machining force analysis and fingerprint reconstruction*

A fingerprint reconstruction of the machined surfaces was carried out using the longitudinal force signal (FL) captured by the dynamometer. Fig. 15 shows the 3D reconstruction of the machining force feedback maps for the standard turning (OD) operation of the sectioned head for all three forging manufacturers. The coordinates of all the

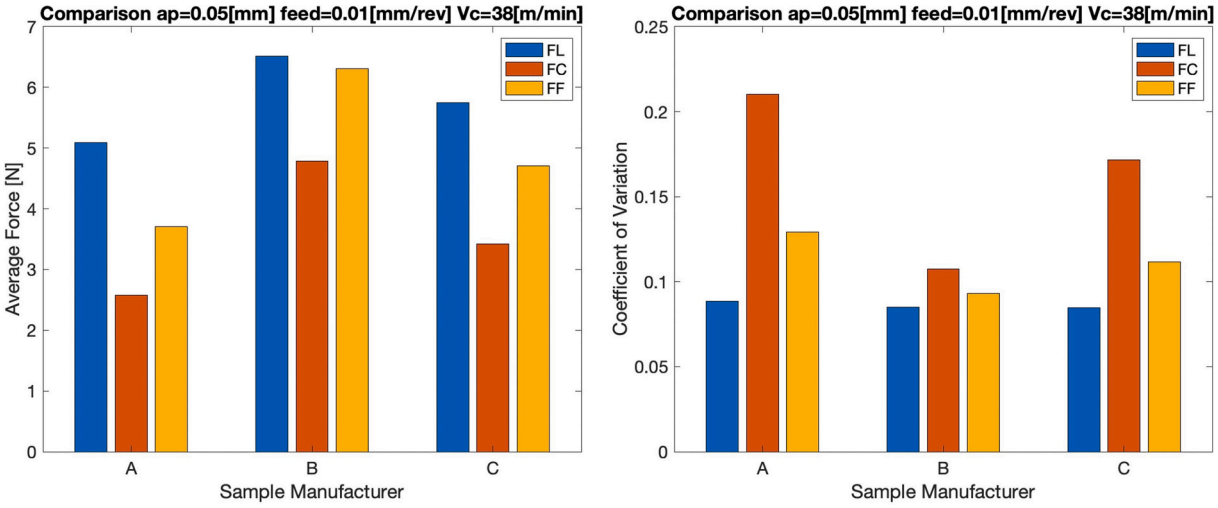

a) *ap=0.05 [mm], feed=0.01 [mm/rev] and Vc=38 [m/min].*

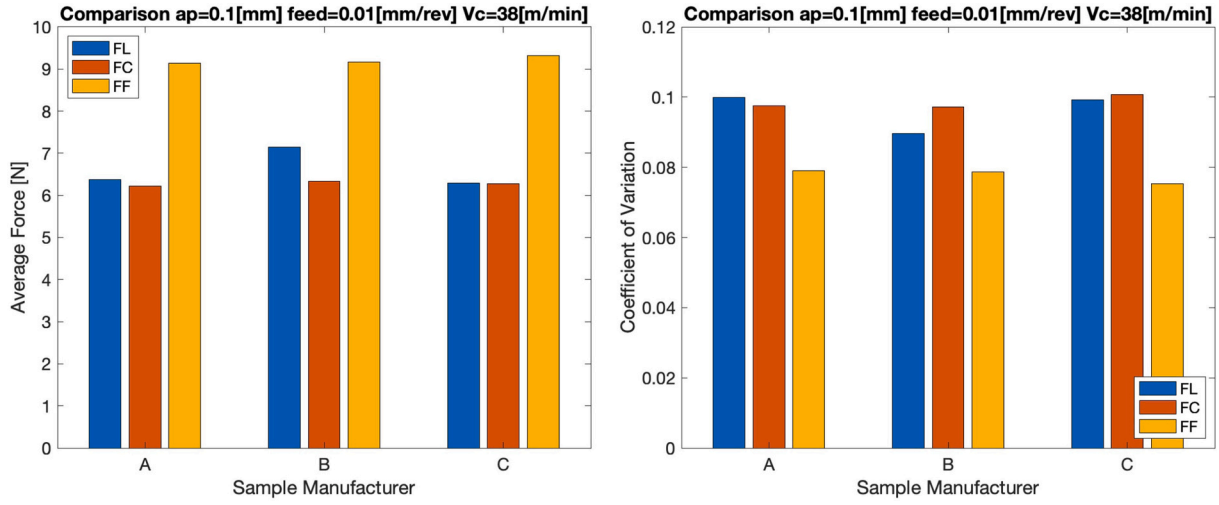

b) *ap=0.1 [mm], feed=0.01 [mm/rev] and Vc=38 [m/min].*

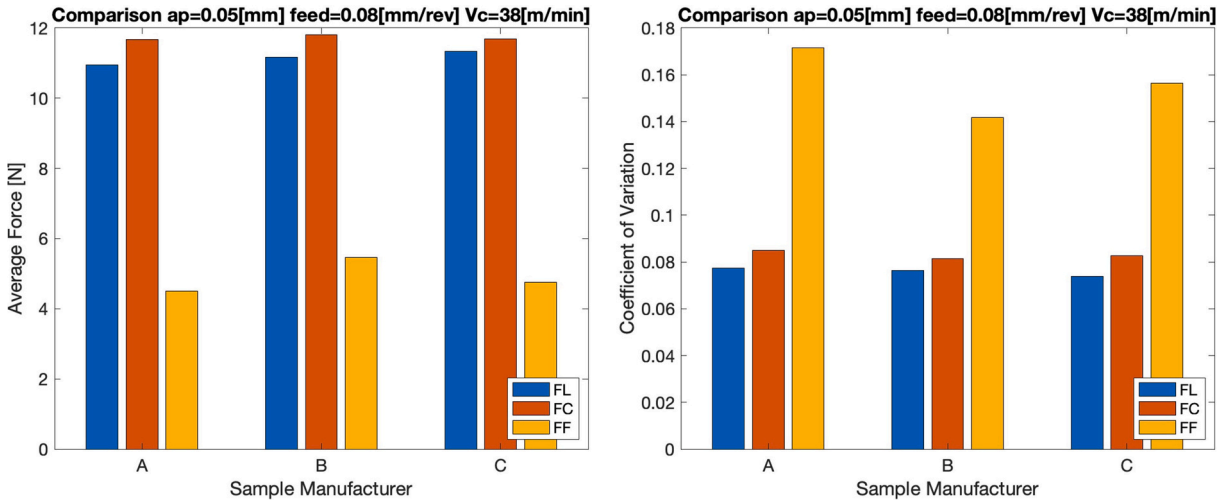

c) *ap=0.05 [mm], feed=0.08 [mm/rev] and Vc=38 [m/min].*

Fig. 14. Statistical analysis results presenting the average measured forces and coefficient of variation for the three forging manufacturers, machining conditions and analysed axes (feed (FF), longitudinal (FL) and cutting (FC)).

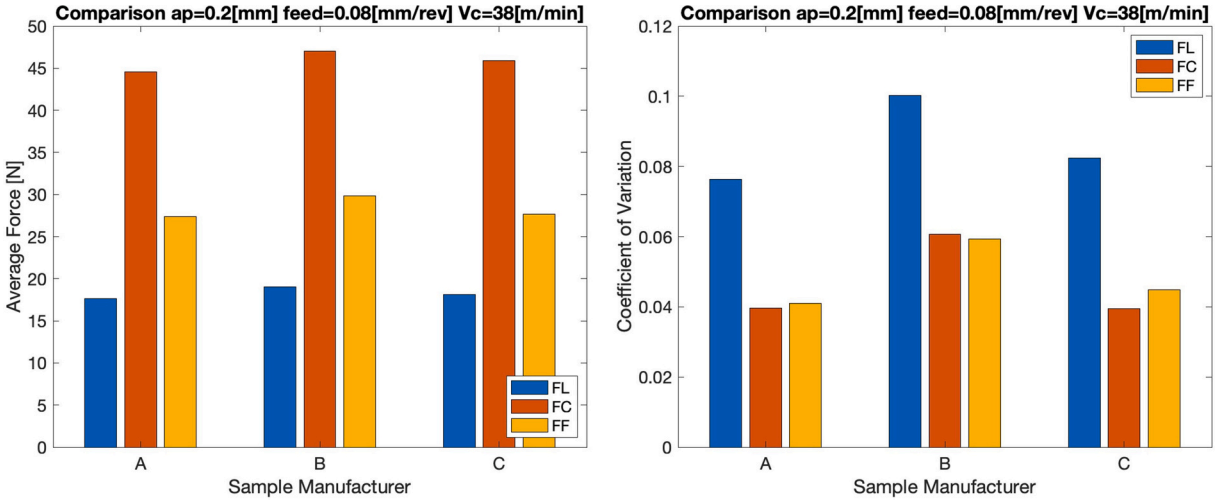

d) *ap=0.2 [mm], feed=0.08 [mm/rev] and Vc=38 [m/min].*

Fig. 14. (*continued*).

reconstructed fingerprint plots in Fig. 15 are the relative position of the tool insert during the machining operation at any given time: the colour scale added to the diagrams is proportional to the FL signal in Newtons measured at those given points. For all the machining trials, the acquisition rate was set to 30 kHz, which means that the spatial resolution of these maps considering the machining parameters used (ap = 0.05 [mm], feed = 0.01 [mm/rev] and Vc = 38 [m/min]) is approximately 1785 pts./rev or 47 pts./mm.

The dark region that appears in the three diagrams is a notch that was scribed into the workpieces (using a hand file), as a reference for the forging plane: this is the reason behind the lower machining forces at the notch location (displayed as dark blue). Moreover, dynamic effects induced by this notch in the first few rotations are also noticeable. This is represented in these diagrams as a distinctive fluctuation in the cutting forces, immediately after the tool crosses the notch. This induced vibration is rooted in the intermittent cutting occurring at this location, however, it quickly dissipates and a steady-state cutting condition is achieved shortly after. Once the notch region is cleared, a complete steady state cutting operation is achieved for the remainder of the machining operation.

The main highlight of these diagrams is the consistent lower forces measured at the forging plane (ND). This is represented as two regions depicted in blue, parallel to the rotational axis of the component and separated by 180 degrees (Fig. 15). Although this is presented in all three (hip joint neck) workpieces, specimen A exhibits a more distinctive banding pattern at the forging plane (Fig. 15 (a)). Specimen C (Fig. 15 (c)) also displays a less prominent change in cutting behaviour at this same location, however, specimen B (Fig. 15 (b)) shows a gentler reduction in force at these locations.

The prominence of these lower cutting force bands, aligned with the ND plane are hypothesized to be influenced by the manufacturer's closed-die forging process, as the symmetry and location of such local machining heterogeneities can only be produced by a manufacturing process whose symmetry axis is in the ND plane.

The effect that is observed in the reconstructed fingerprint plots, where lower cutting forces are found at the ND plane, also correlates with the microstructural plastic instability found in specimen A's stem cross section (Fig. 10a). These local machining heterogeneities are key to understanding the local fatigue performance (and service behaviour) of the hip joint. It is crucial to consider machining as a dynamic process where a crack is purposely created at a given location, mandated by the desired final geometry (depth of cut) at a certain rate (feed) and at a certain speed (cutting speed). This means that the reactions captured by the dynamometer can provide important information about the level of resistance of any specific machining area, and furthermore, infer the local fatigue performance of the machined component. This correlation has been shown by Suarez Fernandez (2020) [21] in titanium alloy forged aerospace components.

3.4.3. *Face turning force analysis and fingerprint reconstruction*

A fingerprint reconstruction was also performed with the longitudinal force captured during the face turning operation of the three analysed hip-joint sectioned heads. A notch was also scribed in the cross section to mark the forging plane and is noticeable in specimens A and B. However, the notch in specimen C was not deep enough to be reconstructed into the fingerprint diagram.

The fingerprint reconstruction using the FL signal captured during the face turning operation for all three manufacturers is shown in Fig. 16. The ND axis is shown parallel to the horizontal axis of the fingerprint graphs, this means that the forging plane is parallel to the Y axis and centred at the origin.

It is important to note, that in the face turning operation, the scribed notch also presents a small disturbance due to the intermittent cut: this is visible to the right of the notch right after the tool edge contacts material again. Moreover, in specimen C, a concentric ring of consistent higher cutting forces is shown. The authors attribute this to a machining dynamic effect, such as chip nesting, rather than a materials effect. This is believed to be the case due to the combination of an extremely thin uncut chip and the continuous change in surface speed, inherent to a face turning operation process at constant RPM.

In this case, the region aligned with the forging plane also shows distinctive cutting behaviour (larger cutting forces) with respect to the rest of the material. This is clear on specimen A, followed by specimen B but is not present in specimen C. Specimen A presents a clear line, however, specimen B shows a cross pattern with two regions in the cross-section of the neck, intersecting at the centre and separated by 10–15°. The authors correlate the prominence of these effects to the lower temperature of the workpiece during the forging operation. Moreover, the geometry of the pattern found could be also attributed to the number of forging blows applied to the component. Specimen B presents a cross pattern, as opposed to a clear distinctive line (similar to specimen A), that could be attributed to a two-blow forging process, in which the workpiece was rotated slightly between forging blows. This is likely to be the case, as the handling of hot preforms is manually performed. However, this hypothesis cannot be validated as the forging parameters were undisclosed by the manufacturers. Finally, the plastic instability

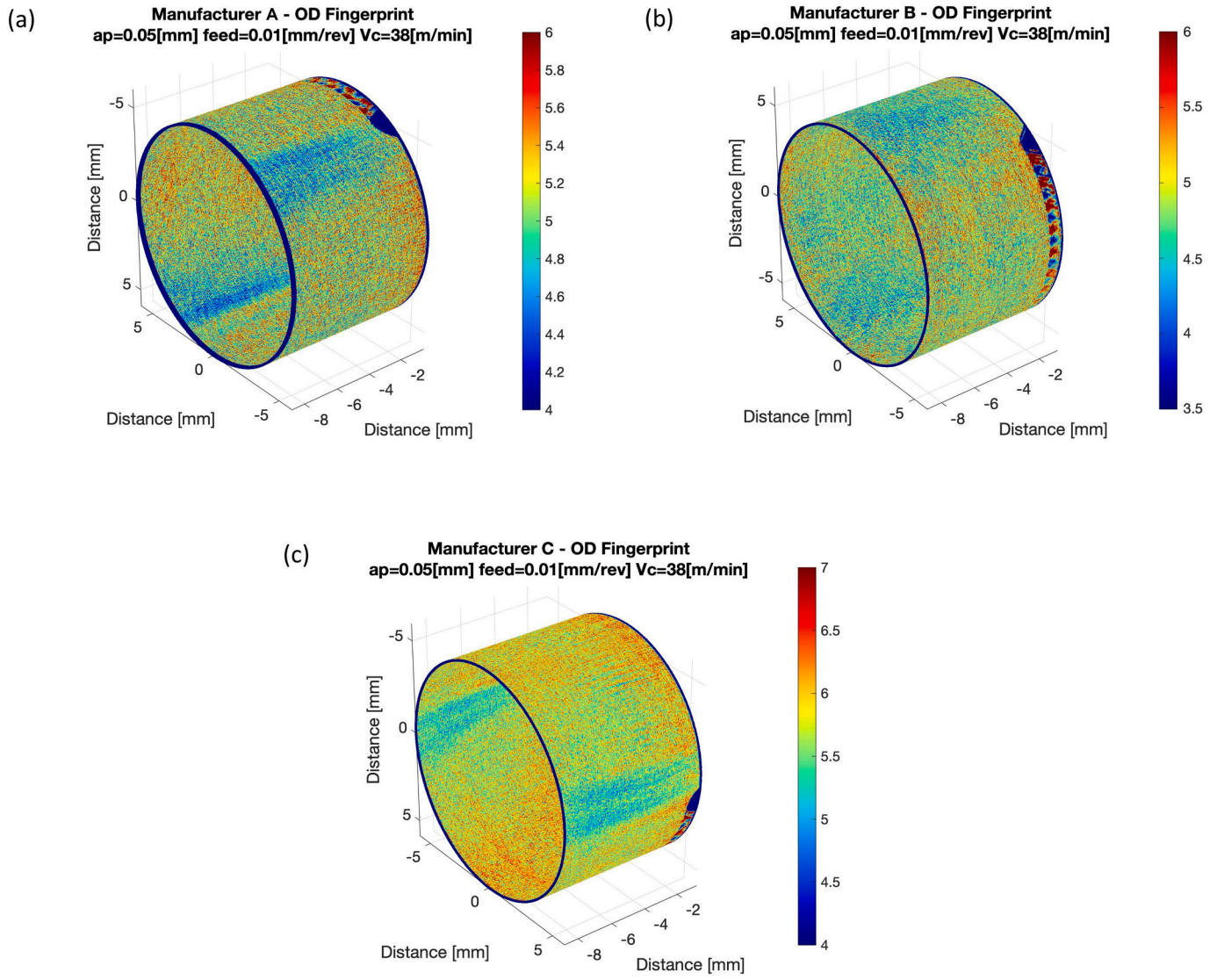

Fig. 15. OD turning fingerprint reconstruction (FL) of the neck for all forging manufacturers A, B and C, ap = 0.05 [mm], feed = 0.01 [mm/rev] and Vc = 38 [m/min] test conditions. 3D fingerprint reconstruction of the machined surface is depicted. The longitudinal axis of the cylinders is aligned with the RD axis.

found in specimen A's cross-section (Fig. 10 (a)) also appears to be affecting the machinability during the face turning operation, resulting in this machining orientation in consistently higher feedback forces.

4. Discussion

4.1. Microstructure vs fatigue performance

The ASTM F136–13 standard states that a bimodal microstructure with non-interconnected α_p grains is required for hip joint applications. Interconnected α_p grains offer low resistance to crack propagation, and therefore, the fatigue performance is reduced [22]. A bimodal microstructure reduces the likelihood of developing interconnected α_p grains, particularly as the volume fraction of α_p grains decreases [23]. In bimodal microstructures, it is generally required to obtain an optimum percentage of α_p grains in order to meet the optimum fatigue performance, since it will also define the α_s colony size, as the smaller the colony size the more resistance to crack propagation [24]. Although a specific volume fraction of α_p grains is not stated by the standard, the processing temperature is stipulated. Titanium alloys, such as Ti-64, are very sensitive to slight variations in the temperature, which leads to a significant effect on the final volume fraction of the α and β phases at room temperature [25]. Therefore, during the NNS forging of hip joints, the importance of temperature control is apparent in order to control the volume fraction of α_p grains and ultimately the fatigue performance.

From the microstructures analysed in this study, it is clear that significant differences occurred during the forging process of these three hip joints, despite the manufacturers A, B and C abiding to the ASTM F136–13 standard [4]. However, no further details are provided regarding the specific thermomechanical processing conditions of these forgings. This provides freedom for each manufacturer to establish their own processing route, which can cause significant differences in the microstructure and final mechanical properties of the component. As previously stated, the processing parameters are temperature, total strain and final geometry for this type of component. Firstly, although the processing temperature is established by the manufacturer, there are several factors that might affect the forging temperature of the component, such as; the temperature of the forging dies; workpiece temperature (for example, the component temperature can reduce significantly if there is a lengthy transfer time from furnace to dies); and the type of furnace and corresponding temperature/time control. Interestingly, none of these factors are considered in the standard. Secondly, the amount of strain applied will depend on the initial preform dimensions, as well as the processing methods utilised during thermomechanical

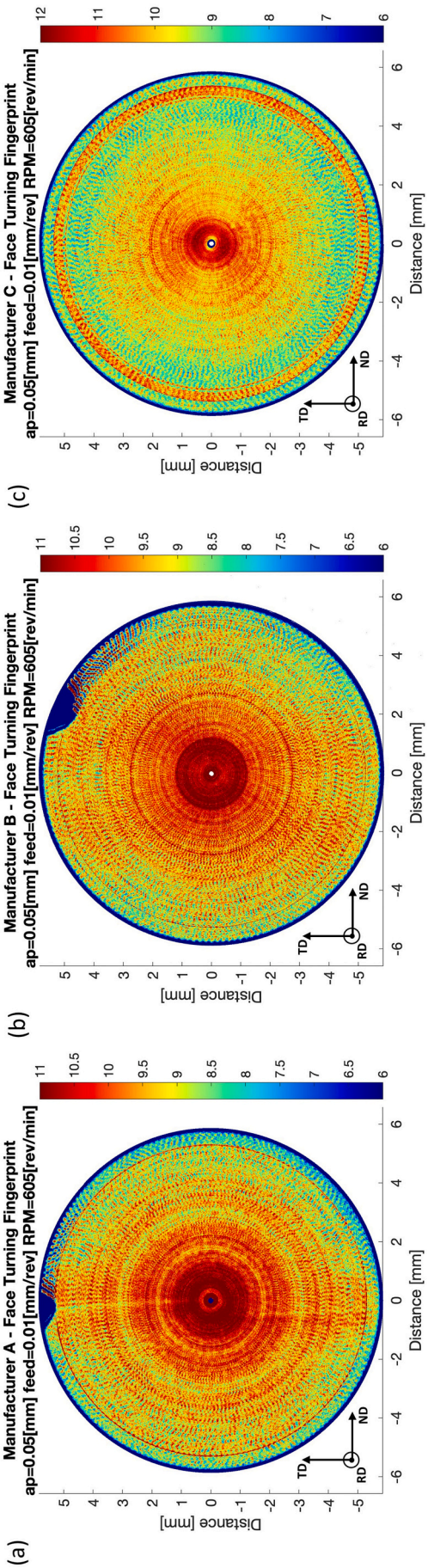

Fig. 16. Face Turning Fingerprint reconstruction (FL) of the head cross section for all three manufacturers, ap = 0.05 [mm], feed = 0.01 [mm/rev] and RPM = 605 [rev/min] test conditions.

processing. Closed-die forging is generally used for the last stage to obtain the final near-net shape before machining, as schematically shown in Fig. 3 (d). However, initial stages involving work on the preform (commonly in bar form), Fig. 3 (a)) prior to closed-die forging, in order to reduce the diameter and bend the bar profile to fit in the closed-die tooling are likely to vary between manufacturers. The initial billet/bar modification process, the number of blows during closed-die forging and the initial preform size will dictate the total amount of strain imparted into the final component. This will determine the final size and morphology of the α_p grains and ultimately the component's behaviour in service. This demonstrates the imperative requirement of considering material quality as the main design variable, as well as the interdependence of the manufacturing process variables on the final component's service integrity.

4.2. Microstructure vs manufacturing process

The microstructure analysis revealed a higher volume fraction of α-phase in specimens A and C which suggests that these forgings were processed at a lower temperature than specimen B. This together with the heavily deformed microstructure at the centre of specimen A, suggests that forging A was processed at the lowest temperature of the three hip joint forgings. Furthermore, the observed defect in specimen A, Fig. 10 (a), is an area of localised deformation commonly identified in forgings as plastic instability which is susceptible to the generation of shear bands. Such features are commonly observed in titanium alloys [26] when high deformation and strain levels are applied at low temperatures. These instabilities are likely to generate intense shear and decohesion in the material due to microvoid formation [27] and hence, lead to premature failure. These defects can occur during isothermal and non-isothermal conditions and are directly related to strain rate and temperature gradients which can lead to further heating and local softening of the material in a positive feedback loop, called 'flow localization' [26]. This effect is rooted in heat that cannot be dissipated during the forging process (due to the poor thermal conductivity of titanium) [28]. Suppressing the formation of such plastic instability features is key, especially when designing hip joints where premature failure implies extra surgical interventions and a severe negative impact on the patient's quality of life.

4.3. Texture vs manufacturing process

The significant similarities of the crystallographic texture found at the edge of the specimens resembles the conventional rolling texture developed in HCP metals [29,30], and can be directly linked to the first stage of the thermomechanical process for these forgings. Even though the exact manufacturing variables and processes for these components cannot be disclosed, it is known that the starting preform materials is generally a bar/cylinder form (as described in section 3.2). This bar undergoes further processing to reduce the diameter via swaging or rotary forging which can theoretically be compared to a standard rolling process, as the forces are applied and the material flows in a specific direction. During this first process, the level of strain applied will play a critical role in the rolling texture strength found in the final component. Therefore, results from the texture analysis suggest that a higher level of strain was applied to specimen C (Fig. 13(f)), compared to A and B, evidenced by the basal {0002} pole figures and corresponding mrd values (Fig. 13(b, d)). Such differences in the texture strength, and therefore in the applied strain, may be caused by variations in the processing temperature, the manufacturing process itself or the starting preform sizes.

The closed-die forging process is used for the second stage during the manufacture of hip joints. This deforms the metal obtaining a NNS component and inducing a strain profile that, for this type of geometry in closed-die forging, normally decreases from centre to edge with respect to the ND axis (Figs. 12 and 13). The area of the component adjacent to

the die experiences the least amount of strain, and therefore, it is likely that the texture present in the preform generated during the first stages during processing, will persist after closed-die forging. Such observations were also found in closed-die forgings for compressor disc manufacture in the aerospace industry at which the texture incoming from billet was still present after closed-die forging at low strain locations [31]. Therefore, the texture at the edge locations is inherited from the first stage during hip joint manufacturing which is weakened or annihilated as strain increases towards the centre of the stem region of the hip forging. The texture analysis revealed an evolution from a prismatic texture with respect to the RD (with most of the c-axis aligned with ND) to a relatively strong basal texture, due to an increase of c-axis crystal aligned with RD (Fig. 12 and Fig. 13). This is the case for the three analysed specimens: specimen C shows the greatest change with most of its HCP crystals rotating 90° evolving from a basal texture (0002)//ND to a (0002)//RD with few low intensity peaks (Fig. 13(e, f)). Consequently, the subtle differences between the edge and the centre, presented in specimens A and B compared to specimen C, suggest some similarities in the manufacturing process of A and B while the processing of C is significantly different. As previously mentioned, for the initial stage such differences can be related to differences in processing temperature, preform size (i.e. initial bar diameter) or the design of the closed-die forging process itself.

The texture analysis performed on the entire half-cross section of the stems from centre to edge revealed that the overall component texture is governed by the texture found at the edge locations: a prismatic texture $\{10\bar{1}0\}$//RD for specimens A and B, and the plane $\{1\bar{2}10\}$//RD for specimen C. Assuming that the texture found at the edge locations is inherited from the first stage of the manufacturing process, these results suggest that the texture generated from the initial process will be preserved, regardless of the nature of the downstream processing variables used during the closed-die forging manufacturing stage. This is due to the fact that during the closed-die forging process only a relatively high amount of strain is achieved at a narrow area in the centre of the stem which is high enough to promote the texture transition mentioned previously. Again, the differences in texture nature as well as in texture evolution between Specimen A, and specimens B and C suggest that: (1) specimen C was processed at the initial stage differently from A and B based on the different prismatic textures found, and (2) specimen C undertakes a higher amount of strain during closed die forging which is revealed by the larger area governed by a basal {0002}//RD texture at the centre. These findings imply that there is a strain threshold at which there is transition in texture (Fig. 17).

4.4. Statistical analysis of machining forces signal (OD turning)

The statistical analysis carried out with data from the steady state, outer diameter (OD) turning operation presents key trends that can be linked to the microstructural developments derived from the prior thermomechanical processing of these workpieces.

It has been shown in previous studies that the differences in machinability response of different forgings can be rooted not only in the chemistry of the workpiece, but also the microstructure condition. This was demonstrated through machining and materials science research carried out by Armendia et al. (2012) [32]. where the machinability of Ti-64, Ti-54M and Ti-6246 was studied by Denkena and Grove [33] with different microstructural variation effects in the response to high precision machining Ti-64 being analysed. Moreover, Telrandhe et al. [34] combined different cutting speeds and Ti-64 microstructures to understand the effects on machinability.

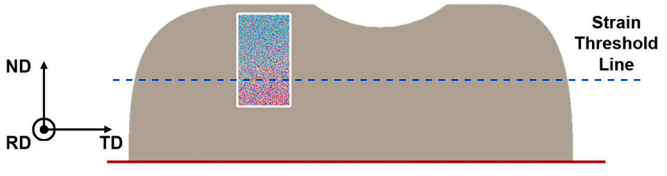

Fig. 17. Theoretical strain threshold line defining potential location of texture transition based on the IPF map with respect to RD of Specimen C.

In this work, the larger average cutting forces are presented by specimen B compared to specimens C and A, respectively. This is because specimen B's microstructure has a higher volume fraction of transformed beta (or secondary alpha) at room temperature compared to the other manufacturers. A higher volume fraction of transformed beta implies higher cutting forces due to an increased chemical interaction between the tool insert and the workpiece, leading to poorer machinability levels [17,32] and enhanced tool wear mechanisms [32]. On the contrary, a larger volume fraction of primary alpha, like that of microstructure in specimen A, results in consistently lower machining forces in comparison, regardless of the machining parameters.

In the case of the coefficient of variation, the lowest variation, and therefore more stable cutting conditions was observed in specimen A: this effect is attributed to its larger alpha content compared to other manufacturers, as well as to its more continuous alpha structure which is a more homogeneous material to cut. On the other hand, specimen B - with lower primary alpha content (due to a higher forging temperature) - presented the largest coefficient of variation. This was reported by Suárez Fernández et al. [17] when comparing the machinability response of different microstructural developments of Ti-6246: microstructures with higher beta content reported larger coefficients of variation. This demonstrates that small percentage changes in the volume fraction of primary alpha and transformed beta (due to the different forging temperatures) can present noticeable differences in the machining response.

However, it is important to note that the relationship between the different manufacturers with respect to the coefficient of variation is inverted when the material removal rate (MMR) is increased. The authors consider that the root of higher coefficient of variation values at low MMRs is the instability in the cutting process due to an extremely thin chip. When the machining variables are in the range of a standard finishing operation for titanium, such instability is suppressed by the thicker chip forming, and therefore the results are more representative of the material that is being machined, rather than being affected by the process.

4.5. Fingerprint reconstruction from machining forces

The force feedback analysis and the fingerprint reconstruction performed in the head region of the implant reveals a localised zone with a distinctive cutting performance with respect to the rest of the machined surface. This region is aligned with the forging plane (ND) and the local material characteristics, texture level and machinability response are believed to be linked to the variables selected during the closed-die forging process.

Moreover, these local machinability fluctuations can be linked to the final local fatigue performance of the component. This is because machining is a dynamic process where a crack is purposely created to achieve a certain geometry. This means that the local response to machining, quantified in this study as the machining forces captured via piezoelectric sensors, can be used to locally infer the material's resistance to develop a crack that can lead to failure [16].

This local heterogeneity found in the local machinability response is in accordance with the results presented in Fig. 12. The local texture developed in the ND plane region during the closed-die forging process presented in specimens A and B consists of a strong basal texture parallel to the longitudinal axis of the head (c-axis // RD // lathe rotation axis). Moreover, the machining response is also influenced by the local texture developed, as demonstrated by Lee et al. [35] for copper crystals and by Lawson et al. [36], in aluminium FCC monocrystals. In the case of titanium alloys, this arises from the inherent anisotropy of the HCP crystal

reported by Zarkades and Larson [37] and the nature of its complex slip system and combinations [38]. This implies a correlation between the local crystallographic texture of the material, the effective slip length and slip transmission in the lattice and the local machining response.

It is important to highlight that the machining heterogeneity measured, that aligns with the ND plane, appears to have the opposite reaction depending on the machining orientation: larger cutting forces are measured in the face turning operation and lower machining resistance during the standard OD turning operation. Although this might seem counterintuitive, it is necessary to consider the crystallographic orientation analysis performed at the instability region and to consider the relative orientation of the crystallographic lattice with respect to the machining forces. Taking this into account and illustrated in Fig. 18, it is possible to observe that the c-axis alignment can produce significant differences in machining response. In the case of the instability found in specimen A (with c-axis // RD), the local machining forces measured at this location, during the face turning operation, were significantly higher than the forces recorded during the standard turning operation. This implies that when the c-axis is parallel to the machining plane, and thus the activation of the slip systems requires more energy resulting in higher forces to remove material.

4.6. Ranking of the forgings from manufacturers from machining response

Based on the materials characterisation analysis presented in this study, manufacturer A is the one that shows the worst forging quality. The large instability found in the ND plane throughout the complete hip joint forging (stem and head) can be linked to premature failure compared to the other two manufacturers. This instability is a defect that can be directly traced to the closed-die forging process. Such instability is derived from a lower than expected forging temperature. Manufacturers B and C do not show any instability at the forging plane (ND) in the microstructural analysis of the cross section of the stem. However, manufacturer B's specimen presents consistently higher cutting forces in the ND plane during the face turning operation. This is not the case with manufacturer C's specimen, where no machining heterogeneities are found in the ND plane. However, during the standard turning operation, all three manufacturers present different levels of lower cutting forces in the ND plane. This is an interesting result, as the microstructural analysis does not reveal such heterogeneity in specimens B and C.

5. Conclusions

This study presents the materials characterisation and response of three hip joints forged by three different manufacturers using a machining force feedback analysis and electron backscatter diffraction. All the analysed specimens were certified and followed all the requirements stated in the previously mentioned standards. This analysis reveals significant heterogeneities and variability between the three manufacturers in microstructure, crystallographic texture development and machinability response - including a case of a plastic instability across the forging plane (ND plane). These types of microstructural features could have significant deleterious effects on the implant's fatigue performance. This implies that the current material and manufacturing standards (and testing) for titanium alloy orthopaedic implants are perhaps not stringent enough, as forgings with severe plastic instability regions can still pass the certified standards.

The authors suggest that additional improvements in process control at manufacturers should be put in place to avoid such microstructural features that could compromise components' performance (and ultimately a patient quality of life) and that research should be focused in minimising microstructure and textural heterogeneities.

Finally, this work has also shown the capabilities of the force feedback analysis to generate microstructural and textural footprints by investigating the cutting forces during machining. The results obtained from standard OD turning and face turning operation indicating a hypothetical orientation of the HCP crystal structure are in agreement with the result from texture analysis using conventional characterisation techniques such as EBSD. Hence, the force feedback technology has shown capabilities to become a promising technique to implement as non-destructive method for qualitative texture analysis on titanium mill products during routine machining operation within a supply chain.

Data availability statement

The raw/processed data and material required to reproduce these findings cannot be shared at this time due to technical or time limitations.

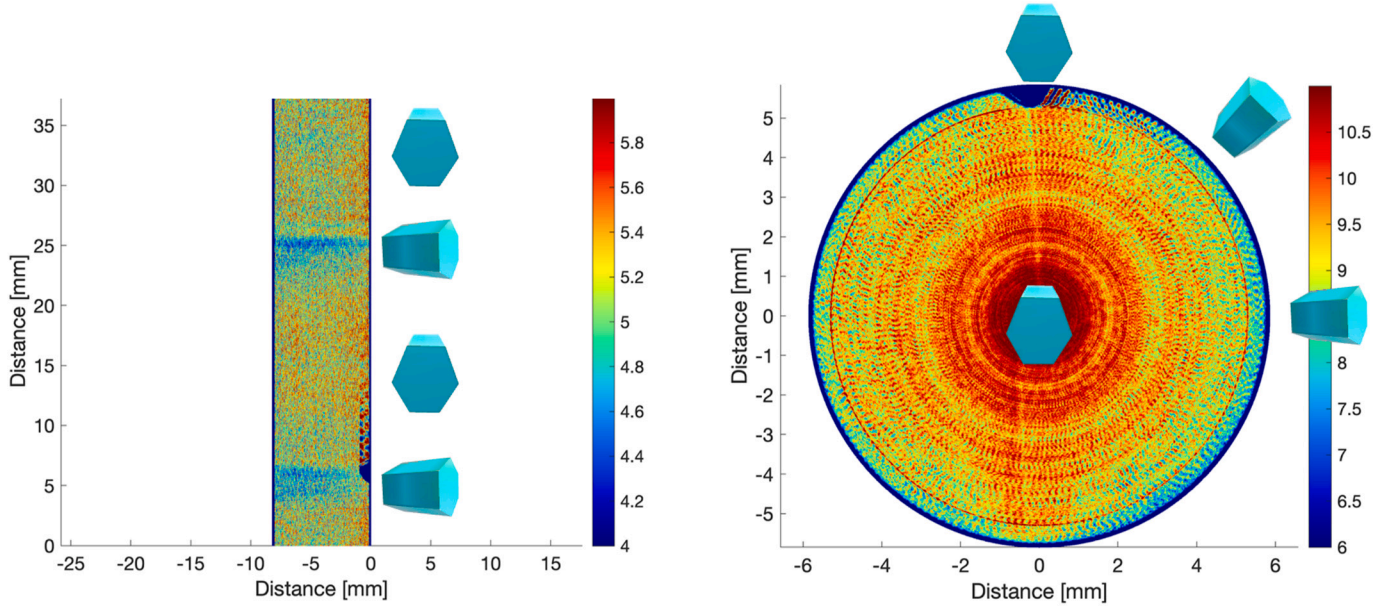

Fig. 18. Schematic representation of the average crystallographic orientation found at the instability location (specimen A) with respect to the reconstructed fingerprint maps from the longitudinal force measured during standard OD turning and face turning operations.

Declaration of Competing Interest

The authors declare that they have no known competing financial interests or personal relationships that could have appeared to influence the work reported in this paper.

Data availability

The authors do not have permission to share data.

Acknowledgements

The authors acknowledge JRI Orthopaedics Ltd. for providing the workpieces characterised and studied in the present work and Oliver Levano Blanch for his support in obtaining large optical micrograph mosaics. This work was supported by the EPSRC [grant EP/S013377/1].

References

[1] S.D. Ulrich, T.M. Seyler, D. Bennett, R.E. Delanois, K.J. Saleh, I. Thongtrangan, M. Kuskowski, E.Y. Cheng, P.F. Sharkey, J. Parvizi, J.B. Stiehl, M.A. Mont, Total hip arthroplasties: what are the reasons for revision? Int. Orthop. 32 (2008) 597–604, https://doi.org/10.1007/s00264-007-0364-3.

[2] C. Delaunay, M. Hamadouche, J. Girard, A. Duhamel, What are the causes for failures of primary hip arthroplasties in France? Clin. Orthop. Relat. Res. 471 (2013) 3863–3869, https://doi.org/10.1007/s11999-013-2935-5.

[3] NJR Report, in: https://reports.njrcentre.org.uk/hips-all-procedures-activity/H03v2NJR?reportid=FFCEA144-54BC-486D-81A6-C6A58DDCA079&defaults=DC_Reporting_Period_Date_Range=%22MAX%22,JYS_Filter_Calendar_Year_From_To=%22min-max%22,R_Filter_Country=%22All%22,H_Fil, 2016.

[4] ASTM F136-13, Standard Specification for Wrought Titanium-6Aluminum-4Vanadium ELI (Extra Low Interstitial) Alloy for Surgical Implant Applications (UNS R56401), 2009, https://doi.org/10.1520/F0136-13.2.

[5] ASTM F620-11, Standard Specification for Titanium Alloy Forgings for Surgical Implants in the Alpha 11, ASTM, 2015, pp. 1–4, https://doi.org/10.1520/F0620-11.2.

[6] ISO, 7206-4:2010, Implants for Surgery — Partial and Total Hip Joint Prostheses Part 4: Determination of Endurance Properties and Performance of Stemmed Femoral Components, International Organization for Standardization, Geneva, Switzerland, 2016, pp. 1–24. http://www.iso.org.

[7] ISO, 7206-6:2013, Implants for Surgery — Partial and Total Hip Joint Prostheses — Part 6: Endurance Properties Testing and Performance Requirements of Neck Region of Stemmed Femoral Components, International Organization for Standardization, Geneva, Switzerland, 2013, pp. 1–26. http://www.iso.org.

[8] ISO 5832-3:2021, Implants for Surgery — Metallic Materials — Part 3: Wrought Titanium 6-Aluminium 4-Vanadium Alloy, (n.d.).

[9] S. Bahl, S. Suwas, K. Chatterjee, The control of crystallographic texture in the use of magnesium as a resorbable biomaterial, RSC Adv. 4 (2014) 55677–55684, https://doi.org/10.1039/c4ra08484e.

[10] Data Protection Act, Data Protection Act 2018. http://Legislation.Gov.Uk, 2018.

[11] W.V. Wood A, R. Denholm, S. Hollings, J. Cooper, S. Ip, Linked electronic health records for research on a nationwide cohort of more than 54 million people in England: data resource BMJ 2021, BMJ 373 (2021).

[12] M.R. Talib, R.J. Toff, Plasma-sprayed coating of hydroxyapatite on metal implants–a review, Med J Malaysia 59 Suppl. B (2004) 153–154.

[13] B.A. Behrens, M. Stonis, T. Blohm, J. Richter, Investigating the effects of cross wedge rolling preforming operation and die forging with flash brakes on forging titanium hip implants, Int. J. Mater. Form. 11 (2018) 67–76, https://doi.org/10.1007/s12289-016-1329-0.

[14] F. Bachmann, R. Hielscher, H. Schaeben, Texture analysis with MTEX- free and open source software toolbox, Solid State Phenom. 160 (2010) 63–68, https://doi.org/10.4028/www.scientific.net/SSP.160.63.

[15] ASTM-E384-17, Standard Test Method for Microindentation Hardness of Materials, (n.d.). doi:https://doi.org/10.1520/E0384-17.

[16] D. Suárez Fernández, M. Jackson, P. Crawforth, K. Fox, B.P. Wynne, Using machining force feedback to quantify grain size in beta titanium, Materialia 13 (2020), https://doi.org/10.1016/j.mtla.2020.100856.

[17] D. Suárez Fernández, B.P. Wynne, P. Crawforth, M. Jackson, Titanium alloy microstructure fingerprint plots from in-process machining, Mater. Sci. Eng. A 811 (2021), https://doi.org/10.1016/j.msea.2021.141074.

[18] S. Cedergren, G. Petti, G. Sjöberg, On the influence of work material microstructure on chip formation, cutting forces and acoustic emission when machining Ti-6Al-4V, Proc. CIRP 12 (2013) 55–60, https://doi.org/10.1016/j.procir.2013.09.011.

[19] B. Denkena, T. Grove, M. Tools, The Effect of Microstructure on the Machinability of Ti-6Al-4V, 2016, pp. 905–910.

[20] X. Chuangwen, D. Jianming, C. Yuzhen, L. Huaiyuan, S. Zhicheng, Jing, The relationships between cutting parameters, tool wear, cutting force and vibration, Adv. Mech. Eng. (2019), https://doi.org/10.1177/1687814017750434.

[21] D. Suárez Fernández, An Assessment of the Effect of Machining and Forging Texture on the Fatigue Performance of Aerospace Titanium Alloys, University of Sheffield, 2020.

[22] J. Everaerts, B. Verlinden, M. Wevers, The influence of the alpha grain size on internal fatigue crack initiation in drawn Ti-6Al-4V wires, Proc. Struct. Integr. 2 (2016) 1055–1062, https://doi.org/10.1016/j.prostr.2016.06.135.

[23] S. Jadhav, A. Powar, S. Patil, A. Supare, B. Farane, R. Singh, Effect of volume fraction of alpha and transformed beta on the high cycle fatigue properties of bimodal Ti6Al4V alloy, IOP Conf. Ser. 201 (2017), https://doi.org/10.1088/1757-899X/201/1/012035.

[24] G. Lutjering, Influence of processing on microstructure and mechanical properties of (α+β) titanium alloys, Mater. Sci. Eng. A 243 (1998) 32–45, https://doi.org/10.1016/S0921-5093(97)00778-8.

[25] H.M. Flower, Microstructural development in relation to hot working of titanium alloys, Mater. Sci. Technol. 6 (1990) 1082–1092, https://doi.org/10.1179/mst.1990.6.11.1082.

[26] S.L. Semiatin, G.D. Lahoti, S.I. Oh, The occurrence of shear bands in metalworking, in: J. Mescall, V. Weiss (Eds.), Material Behavior under High Stress and Ultrahigh Loading Rates, Springer US, Boston, MA, 1983, pp. 119–159, https://doi.org/10.1007/978-1-4613-3787-4_7.

[27] J.J.J.S.L. Semiatin, Formability and workability of metals: plastic instability and flow localization, volume 2 o, Am. Soc. Metals (1984) 1984.

[28] T.J. Burns, M.A. Davies, On repeated adiabatic shear band formation during high-speed machining, Int. J. Plast. 18 (2002) 487–506, https://doi.org/10.1016/S0749-6419(01)00006-7.

[29] Y.N. Wang, J.C. Huang, Texture analysis in hexagonal materials, Mater. Chem. Phys. 81 (2003) 11–26, https://doi.org/10.1016/S0254-0584(03)00168-8.

[30] J. Zhao, L. Lv, G. Liu, Experimental and simulated analysis of texture evolution of TA15 titanium alloy sheet during hot tensile deformation at 750°C, Proc. Eng. 207 (2017) 2179–2184, https://doi.org/10.1016/j.proeng.2017.10.978.

[31] N. Gey, P. Bocher, E. Uta, L. Germain, M. Humbert, Texture and microtexture variations in a near-α titanium forged disk of bimodal microstructure, Acta Mater. (2012), https://doi.org/10.1016/j.actamat.2012.01.031.

[32] M. Armendia, P. Osborne, A. Garay, J. Belloso, S. Turner, P.J. Arrazola, Influence of heat treatment on the machinability of titanium alloys, Mater. Manuf. Process. 27 (2012) 457–461, https://doi.org/10.1080/10426914.2011.585499.

[33] T. Denkena, B. Grove, The effect of microstructure on the machinability of Ti-6Al-4V, in: Proceedings of the 13th World Conference on Titanium, 2016, https://doi.org/10.1002/9781119296126.ch155.

[34] S.V. Telrandhe, A.K. Saxena, S. Mishra, Effect of microstructure and cutting speed on machining behavior of Ti6Al4V alloy, J. Mech. Sci. Technol. 31 (2017) 2177–2184, https://doi.org/10.1007/s12206-017-0413-9.

[35] W.B. Lee, S. To, C.F. Cheung, Effect of crystallographic orientation in diamond turning of copper single crystals, Scr. Mater. 42 (2000) 937–945, https://doi.org/10.1016/S1359-6462(00)00329-8.

[36] B.L. Lawson, N. Kota, O.B. Ozdoganlar, Effects of crystallography anistropy on orthogonal micromachining of single-crystal aluminum, J. Manuf. Sci. Eng. Trans. ASME 130 (2008) 0311161–03111611, https://doi.org/10.1115/1.2917268.

[37] A. Zarkades, F.R. Larson, Elasticity of titanium sheet alloys, in: N.E.P.R.I. Jaffee (Ed.), The Science, Technology and Application of Titanium, Pergamon Press Ltd, 1970, pp. 933–941.

[38] T.B. Britton, F.P.E. Dunne, A.J. Wilkinson, On the mechanistic basis of deformation at the microscale in hexagonal close-packed metals, Proc. R. Soc. A 471 (2015), https://doi.org/10.1098/rspa.2014.0881.